Physics – Uspekhi **57** (10) 959 – 969 (2014)

REVIEWS OF TOPICAL PROBLEMS PACS numbers: **72.40.+w**, 73.20.Hb

Terahertz photoconductivity and nontrivial local electronic states in doped lead telluride-based semiconductors

L I Ryabova, D R Khokhlov

DOI: 10.3367/UFNe.0184.201410b.1033

Contents

Abstract. This paper reviews unusual photoelectric effects observed in doped narrow-gap PbTe-based semiconductors exposed to intense terahertz laser pulses. It is shown that in some cases these effects are due to those (nontrivial) local electronic states that, unlike ordinary, spectrally defined impurity states, are linked to the quasi-Fermi level, whose position can be varied by changing the degree of photoexcitation.

1. Introduction

The list of demanded functional properties of semiconductors is continuously widening. This natural process is determined both by expanding the scope of various practical applications and the refinement of technologies and the development of theoretical concepts revealing new aspects in the study and applications of known semiconductors. As applied to lead chalcogenide-based solid solutions, an example is the prediction [1] and subsequent experimental observation [2, 3] of topological phases on the surface of samples with the inversed spectral structure. Particular interest in doped lead telluride as a thermoelectric material is motivated by the specific features of impurity states, forming in a number of cases energy levels (or impurity bands) with a high electron density against the background of allowed energies. Calculations [4] have demonstrated that the delta-like shape of the density-of-states function leads to an increase in the thermoelectric Q-factor. This conclusion was experimentally confirmed in numerous recent studies, in particular, those devoted to the study of PbTe(Tl) and PbTe(In) [5–8]. The preparation of lead chalcogenides in the form of colloidal nanocrystals is promising for their use in solar batteries [9]. Nevertheless, one of the main applications of these solid solutions concerns optoelectronics.

Traditionally, lead chalcogenide-based solid solutions have been considered as promising materials for photodetectors and infrared (IR) lasers [10, 11]. However, the unique properties of some impurities [12–14] considerably changed the notion of the spectral-sensitivity range of doped $Pb_{1-x}Sn_xTe(In)$. In this review, we discuss studies of the photoconductivity of doped $Pb_{1-x}Sn_xTe$ solid solutions in the terahertz spectral range.

The paper outline is as follows. The main material of the review is presented in Sections 2–5. Section 2 is devoted to the properties of $Pb_{0.75}Sn_{0.25}Te(In)$ single crystals. The choice of the composition $x = 0.25$ and indium as a dopant is not accidental, being determined by the energy level diagram. The peculiarities of the formation of impurity states in $Pb_{1-x}Sn_xTe(In)$ solid solutions are caused by the correlation interaction in the impurity center/nearest crystal environment and, as a result, by a variable valence of the impurity [14, 15]. The presence of a few charge states of the impurity atom leads to the formation of a system of impurity levels, stabilization of the Fermi-level location, and the emergence of long-term relaxation processes of electronic distributions at low temperatures, and possibly, to the persistent photoconductivity.

Figure 1 shows a reconstruction diagram of the energy spectrum of indium-doped lead telluride–tin telluride alloys [16]. The stabilized Fermi level is shifted down along the

L I Ryabova Faculty of Chemistry, Lomonosov Moscow State University, Leninskie gory 1, str. 3, 119991 Moscow, Russian Federation
Tel. +7 (495) 939 11 51
E-mail: mila@mig.phys.msu.ru
D R Khokhlov Faculty of Physics, Lomonosov Moscow State University, Leninskie Gory 1, str. 2, 119991 Moscow, Russian Federation;
Lebedev Physical Institute, Russian Academy of Sciences, Leninskii prosp. 53, 119991 Moscow, Russian Federation
Tel. +7 (495) 938 11 51
E-mail: khokhlov@mig.phys.msu.ru

Received 15 January 2014, revised 8 February 2014
Uspekhi Fizicheskikh Nauk **184** (10) 1033 – 1044 (2014)
DOI: 10.3367/UFNr.0184.201410b.1033
Translated by M Sapozhnikov; edited by A Radzig

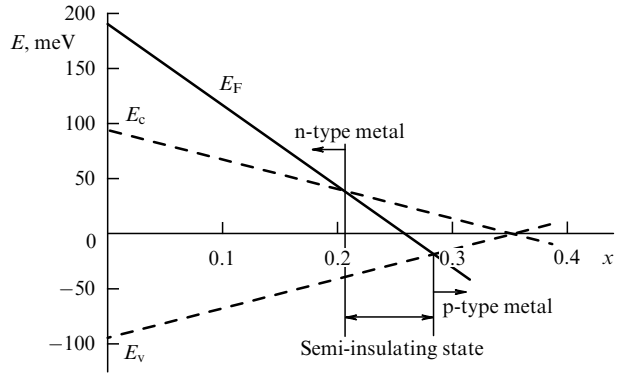

Figure 1. Energy-spectrum reconstruction diagram for solid solutions $Pb_{1-x}Sn_xTe(In)$ under changes of composition x [16].

energy scale as the mole fraction x of tin telluride in the alloy increases, and at $x = 0.25$ the Fermi level is located 20 meV below the conduction band bottom, ensuring the formation of a semi-insulating state at low temperatures.

High concentrations of free charge carriers in undoped solid $Pb_{1-x}Sn_xTe$ solutions caused by intrinsic electrically active defects have considerably restricted the possibility of using this material for manufacturing photodetectors. The preparation of semi-insulating solid solutions stimulated the study of photoconductivity in this material. Studies in the terahertz spectral range were initiated by the experimental result [17], according to which solid solutions of this composition proved to be sensitive to photon energies much lower than 20 meV. The photoconductivity was observed up to a radiation wavelength of 241 μm, which exceeds the long-wavelength threshold $\lambda = 220$ μm of photoeffect for uniaxially stressed Ge(Ga) [18], which was considered maximal for highly sensitive photodetectors.

Experimental investigations of the photoconductivity of $Pb_{0.75}Sn_{0.25}Te(In)$ single crystals in the terahertz range revealed that the photoconductivity of these materials is determined by a new type of impurity states, whereas the long-wavelength threshold of photoconductivity is virtually absent [19]. This result stimulated the study of photoconductivity in the terahertz region in strongly degenerate PbTe(In). Section 3 is devoted to the study of terahertz photoconductivity in PbTe(In) films with a variable microstructure. In Section 4, we discuss the influence of a magnetic field and electric current on the character of terahertz photoconductivity in $Pb_{1-x}Sn_xTe(In)$ with a variable composition x.

Indium is not a sole dopant providing the photoconductivity of lead telluride in the terahertz spectral range. Section 5 is concerned with the consideration of terahertz photoconductivity in lead telluride doped with gallium and vanadium.

In concluding Section 6, we discuss the outlook for practical applications of the materials under study as photosensitive sensors in the IR and terahertz spectral ranges.

2. Semi-insulating solid solutions $Pb_{0.75}Sn_{0.25}Te(In)$

The spectroscopy of photoelectric characteristics, in particular, photoconductivity, is one of the basic experimental techniques for determining the location of energy levels in semiconductor spectrum. At the same time, the direct application of such techniques to materials with persistent photoconduction is quite complicated: standard cryogenic spectral equipment does not shield a sample from the background radiation inherent in any spectrometer. However, if a semiconductor exhibits persistent photoconductivity, this background radiation will excite many nonequilibrium charge carriers in the sample during its cooling already before the beginning of the experiment, and therefore the experiment cannot be started from the ground 'dark' state. This problem is even more aggravated for narrow-gap group IV–VI semiconductors, because the characteristic energies of their spectra are lower than those for wide-gap semiconductors; therefore, room background radiation acts more efficiently.

Photoelectric phenomena in materials with persistent photoconductivity can be studied by two methods. The first one, so-called low-background, assumes the total shielding of a sample from thermal background radiation. A disadvantage of the low-background approach is the formation of a complicated spectrum of radiation incident on the sample and the subsequent complexity of determining the spectral characteristics of a photodetector.

To overcome this disadvantage, the high-background method is applied when the sample is not shielded from background radiation. In this case, external radiation sources with a calibrated intensity and spectrum can be used. However, they should be high-powerful enough to obtain a photoresponse amplitude noticeable against the background signal from free nonequilibrium charge carriers excited by background radiation. This approach was applied to analyze the mechanisms of photoconductivity in $Pb_{1-x}Sn_xTe(In)$ irradiated by high-power 100-ns laser pulses at 90, 148, 280, and 496 μm [20, 21]. The laser radiation power was controlled with a photon avalanche detector [22]. The typical diameter of a laser beam was 1–3 mm. Measurements with a pyroelectric camera revealed that the laser beam had virtually a Gaussian shape [23]. The measurement technique is described in detail in papers [20, 21, 24].

Background irradiation in $Pb_{0.75}Sn_{0..25}Te(In)$ single crystals provided an increase by more than four orders of magnitude in their conductivity compared to that in the dark state [25]. Nevertheless, irradiation by laser pulses at different wavelengths even in the presence of this background radiation induced a strong photoconductivity signal $\Delta\sigma$. Depending on experimental conditions, the photoresponse could be either positive or negative. At low temperatures, the positive photoconductivity with characteristic relaxation times considerably exceeding the laser pulse duration dominates. As the temperature is increased, the sign of the signal changes to negative, and the kinetics of $\Delta\sigma$ repeat the time profile of the laser pulse (Fig. 2) [24, 25].

Considerable differences in the type of change in the amplitudes of negative and positive signals $\Delta\sigma$ were found when the incident radiation power was varied with the help of attenuators inserted into the laser beam. The dependences of $\Delta\sigma(N)/\sigma_0$ (σ_0 is the initial photoconductivity at a given temperature) on the number N of photons incident on a sample per unit time in the case of positive photoconductivity ($T = 4.2$ K) are substantially different for different incident radiation wavelengths. In the case of negative photoconductivity ($T = 25$ K), experimental points for different excitation wavelengths fall, in fact, on the same curve, at least in the region of small N. This means that the formation mechanisms of the positive and negative photoresponses are distinct. The negative photoresponse observed at higher temperatures is

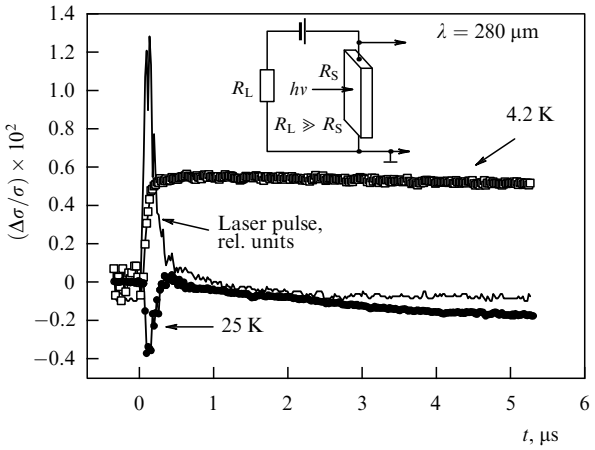

Figure 2. Kinetics of the photoconductivity $\Delta\sigma/\sigma$ in a $Pb_{0.75}Sn_{0.25}Te(In)$ sample irradiated by a 280-μm laser pulse at different temperatures. The inset shows the measurement circuit: R_L is the load resistance, and R_S is the sample resistance [25].

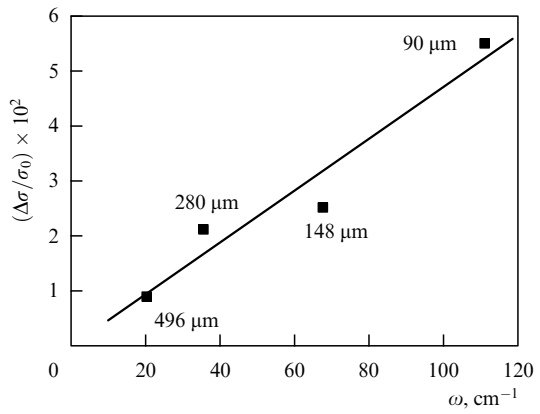

Figure 4. Dependence of the photoconductivity amplitude $\Delta\sigma/\sigma_0$ on the incident radiation frequency ω for the fixed photon flux density $N = 6 \times 10^{23}$ s^{-1} at $T = 4.2$ K [24].

probably caused by the heating of free charge carriers by the laser pulse, resulting in a decrease in their mobility at invariable concentration [24].

Measurements of the Hall voltage kinetics during irradiation by laser pulses in magnetic fields with different strengths [26] confirmed the previous assumption [25] that the low-temperature persistent photoconductivity is caused by the generation of nonequilibrium charge carriers (Fig. 3). Thus, the positive photoconductivity of $Pb_{0.75}Sn_{0.25}Te(In)$ for $T < 10$ K is in compliance with the operation principle of photon radiation detectors. The long-wavelength threshold of the photoeffect for this detector exceeds 496 μm. Moreover, available experimental data give grounds to assume that the ionization energy of metastable impurity states is close to zero.

Figure 4 demonstrates the dependence of $\Delta\sigma/\sigma_0$ on the incident radiation frequency ω for a fixed photon flux density $N = 6 \times 10^{23}$ s^{-1} at 4.2 K, i.e., for positive persistent photoconductivity. The dependence $\Delta\sigma/\sigma_0(\omega)$ is close to linear one. Extrapolation by a straight line drawn through experimental points by the method of least squares to the zero signal $\Delta\sigma = 0$ gives a nearly zero frequency.

The virtual absence of the long-wavelength threshold of the photoeffect is also confirmed by another important argument. All experiments in the terahertz region were performed with background irradiation of samples providing a concentration of nonequilibrium charge carriers of order 10^{17} cm^{-3}. This corresponds to the location of the quasi-Fermi level by ~ 10 meV above the conduction band bottom. This value considerably exceeds the laser photon energy of 2.5 meV (wavelength 496 μm), 4.4 meV (280 μm), and even 8.4 meV (148 μm). Therefore, local states responsible for the appearance of positive persistent photoconductivity should be separated from the quasi-Fermi level by no more than 2.5 meV.

Studies of degenerate semiconducting n-PbTe(In) films confirmed that the terahertz photosensitivity of solid $Pb_{1-x}Sn_xTe(In)$ solutions are provided by some specific local electronic states resided near the quasi-Fermi level [19, 27].

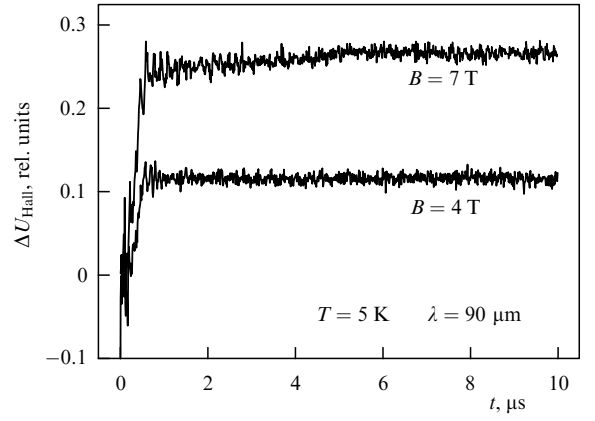

Figure 3. Kinetics of the photoelectric Hall effect in magnetic fields 4 and 7 T at 5 K upon laser excitation at 90 μm [26].

3. PbTe(In) films

In indium-doped lead telluride, the Fermi level is stabilized by 70 meV above the conduction band bottom. The electron concentration reaches 6×10^{18} cm^{-3}, providing a high degree of degeneracy of the electron gas and a high low-temperature conductivity of samples. To study the photoconductivity of PbTe(In) samples, it is preferable to invoke films because they provide more uniform photoexcitation over the volume and more intense signals.

3.1 Influence of the microstructure on transport properties

The conductivity and photosensitivity of semiconducting films are determined by both volume and surface states, and in the case of polycrystalline films also by the peculiarities of the formation of intercrystallite boundaries [28, 29]. By changing the microstructure, we can change the type and character of conductivity, induce a persistent photoconductivity, and exert influence on the temperature of its appearance. All these processes have been observed in nano- and polycrystalline indium-doped lead telluride-based films [30–34]. The character of the photoconductivity in PbTe(In) films in the terahertz spectral region also proved to be quite sensitive to their microstructure [35].

The films under study can be conventionally divided into two groups: nanocrystalline films with grain diameters smaller than 200 nm, and polycrystalline ones with grain

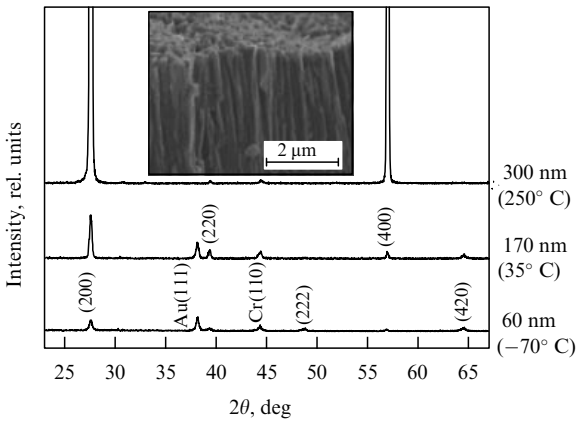

Figure 5. X-ray diffraction spectra of PbTe(In) films. The size of grains and substrate temperature during synthesis are shown alongside the curves. The Au and Cr peaks are related to contacts. The inset shows a high-resolution electron-microscope image of the film [36].

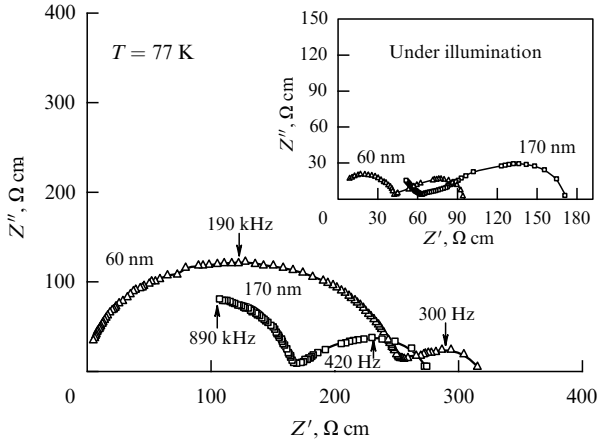

Figure 7. Impedance spectra of PbTe(In) films taken under conditions of shielding and illumination (see inset). The grain size is marked alongside the curves, and $T = 77$ K [36].

diameters larger than 300 nm. Figure 5 displays X-ray diffraction spectra of films of both types and a high-resolution electron microscope image of the film section throughout the depth. All the films have a columnar structure with the columns oriented perpendicular to the substrate plane (in this case, the column diameter is taken as the crystallite size). However, columns in nanocrystalline films have no predominant crystallographic orientation, whereas polycrystalline films exhibit a distinct texture — a distinguished crystallographic direction. The appearance of the texture is accompanied by a change from hole to electron type conduction and a qualitative change in the transport mechanism of charge carriers [36].

The temperature dependences of the electric conduction of nanocrystalline films are characterized by the presence of the activation region at high temperatures and the appearance of persistent photoconductivity for $T > 150$ K (Fig. 6). These effects are in noway related to the bulk properties of PbTe(In) grains, but are due to the formation of inversion channels with the hole conduction on their surface [28, 32, 37, 38]. Intercrystallite barriers appearing in the process provide modulation of the band relief. Activation segments in the temperature dependences of the conductivity are determined by the activation energy for the mobility threshold, while the persistent photoconductivity by recombination barriers appearing due to the spatial separation of nonequilibrium charge carriers.

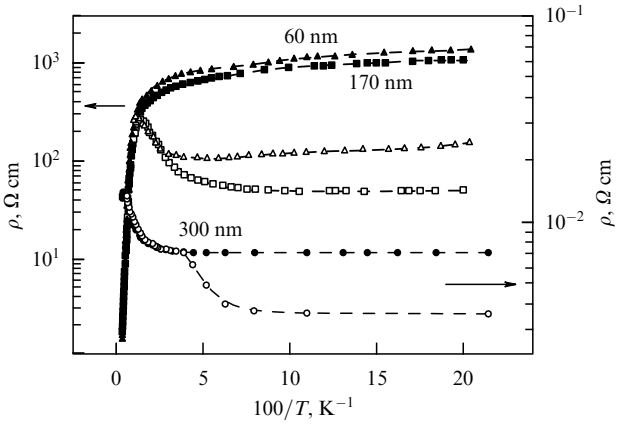

Figure 6. Temperature dependences of the resistivity of PbTe(In) films. The grain size d is shown alongside the curves. Closed symbols correspond to measurements in the case of shielding, the open ones are measurements during illumination with a miniature incandescent lamp [36].

That the carrier transport in nanocrystalline films depends precisely on structural features is confirmed by the frequency dependences of components of the total impedance [32–38]. Figure 7 illustrates the impedance spectra (dependences of the imaginary part Z'' of the impedance on its real part Z', where a variable parameter is frequency f) of p-type films with different grain sizes, measured at 77 K with shielding from background radiation. The inset shows the impedance spectra of the same films measured with illumination by white light from a miniature incandescent lamp placed directly into the measurement chamber.

The impedance spectra clearly exhibit two frequency-resolved branches. This points to the fact that the conductivity of samples is determined by contributions from two transport mechanisms: one of which dominates in the low-frequency region, and the other in the high-frequency region. In the dark, each of the branches is close to a semicircle, corresponding to an equivalent circuit consisting of two parallel RC chains with frequency-independent parameters R (resistance) and C (capacitance). Analysis of the frequency dependences of components of the total impedance and impedance spectra of samples in the equivalent-circuit context showed that the low-frequency branch corresponds to the charge transport along inversion channels on the surface of grains, whereas the high-frequency branch corresponds to transfer over intercrystallite barriers [32]. This conclusion is confirmed by the fact that the calculated capacitance for the low-frequency branch exceeds the capacitance corresponding to the high-frequency semicircle of the impedance spectrum by more than three orders of magnitude. Such high values of the low-frequency capacitance can be provided by a branched network of inversion channels on the surfaces of grains [28, 29]. The resistance corresponding to the high-frequency branch drastically decreases in the presence of background irradiation. Such a process is associated with a decrease in the height of intercrystallite barriers during the generation of nonequilibrium carriers.

The increase in the crystallite site and the appearance of the distinguished crystallographic direction in the orientation of grains in n-type PbTe(In) films is accompanied by the appearance of properties similar to those of single-crystal samples [39]. The temperature dependence of the conductivity of such films is typical for degenerate semiconductors (see Fig. 6), the conductivity being so low that it is impossible to take an informative impedance spectrum. As in PbTe(In) single crystals, the persistent conductivity in n-type films emerges at temperatures below 25 K [36]. All this suggests that the transport of carriers and the photoconductivity of polycrystalline films determine the crystallite bulk characterized by stable electrophysical parameters and a stable location of the Fermi level. Studies of the photoconductivity in the terahertz spectral region have shown that the kinetics and even the sign of a photoresponse are different for nano- and polycrystalline films [27, 35, 40].

3.2 Photoconductivity in the terahertz spectral range

Photoconductivity in the terahertz spectral range was studied for films with grains 60 nm (nanocrystalline films with properties determined by the modulation of the band relief) [35] and 300 nm (analogs of PbTe(In) single crystal samples) [27, 40] in size. Noticeable photoresponses were observed in all films irradiated by laser pulses at 90, 148, and 280 μm in the entire temperature range under study, $T \leqslant 150$ K.

Unlike single-crystal $Pb_{1-x}Sn_xTe(In)$ samples, the photoresponse of nanocrystalline PbTe(In) films is negative in the entire temperature range. The photoconductivity kinetics exhibit persistent behavior, which is especially pronounced at low temperatures (Fig. 8).

Positive terahertz photoconductivity with the same characteristic features as in $Pb_{1-x}Sn_xTe(In)$ single crystals was revealed in PbTe(In) films with grains 300 nm in size. Figure 9 shows typical kinetic curves for the relative photoconductivity of a PbTe(In) film irradiated by laser pulses at different wavelengths. Dashed curves in this figure depict time dependences of the total energy (integrated power) for each laser pulse. The almost complete coincidence of the $\Delta\sigma/\sigma_0(t)$ dependences with the total pulse energy indicates that a polycrystalline film is a variant of an integrating radiation detector.

Background irradiation during experiments leads to twice as much conductivity in a polycrystalline film as that in the absence of this radiation. This corresponds to an increase in electron concentration up to 1.2×10^{19} cm^{-3} and the increase in Fermi energy by ~ 30 meV with respect to its value in the

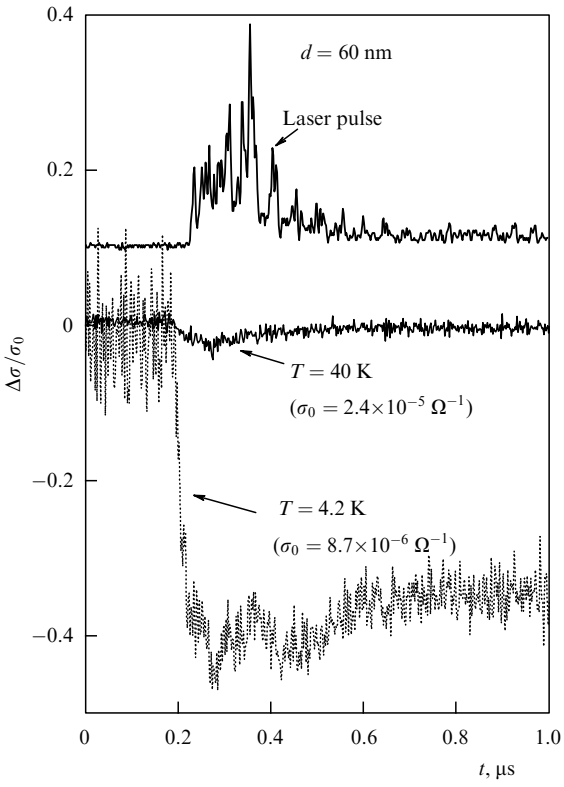

Figure 8. Changes in the relative photoconductivity of a PbTe(In) film with a grain size of 60 nm during the propagation of a 280-μm laser pulse at different temperatures [35].

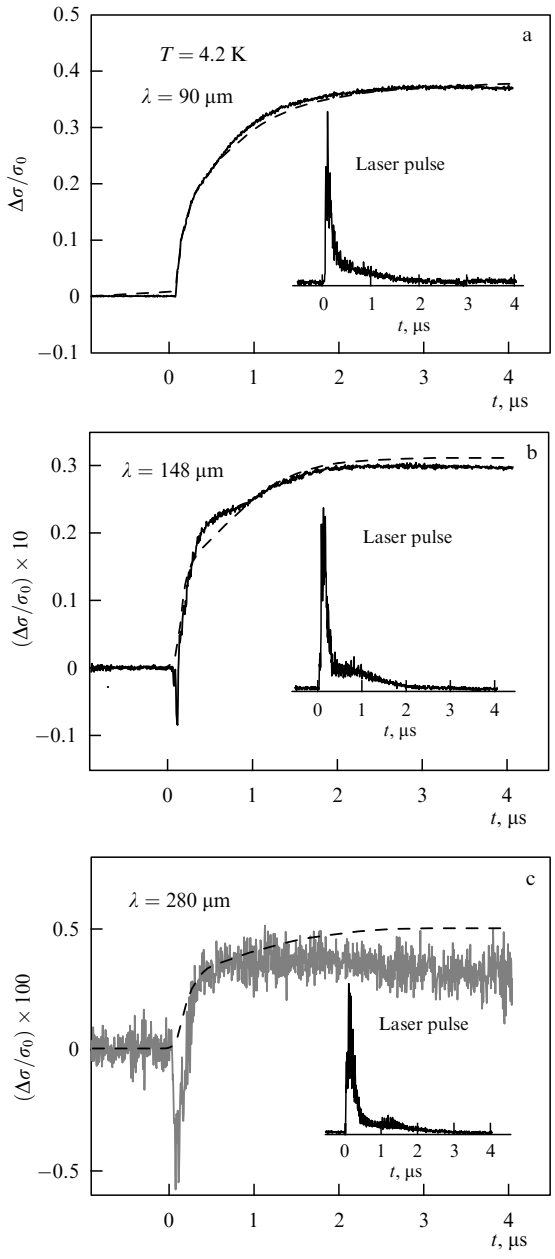

Figure 9. Photoconductivity kinetics in a polycrystalline PbTe(In) film with the grain size $d = 300$ nm during the propagation of 90-μm (a), 148-μm (b), and 280-μm (c) laser pulses at 4.2 K. Time profiles of laser pulses are shown in the insets. The integrated power of laser pulses (total pulse energy) is shown by dashed curves [40].

equilibrium dark state. Before the propagation of a laser pulse, the quasi-Fermi level is located ~ 100 meV above the conduction band bottom. Nevertheless, a noticeable photoresponse is observed for a photon energy lower than 10 meV. This precludes the possibility of photoexcitation of charge carriers from the impurity level stabilizing the Fermi level location. In fact, a fraction of electrons with energies close to the quasi-Fermi level energy does not contribute to transport processes without additional activation. It is important to note that photoconductivity induced by terahertz irradiation, like photoconductivity in the presence of background irradiation, is persistent. In addition, the positive photoresponse cannot be caused by a change in mobility due to electron-gas heating. Therefore, laser pulses promote generation of long-lived majority charge carriers.

The fact that excitation of electrons by a terahertz laser pulse is related to the states 'linked' to the position of the quasi-Fermi level was most conclusively confirmed in the experimental study of the kinetics of terahertz photoconductivity in PbTe(In) films by varying the location of the quasi-Fermi level [27].

The energy of the quasi-Fermi level was additionally increased by pumping nonequilibrium charge carriers with series of laser pulses. After sample cooling in the presence of background irradiation, a series of 200 90-μm laser pulses was applied. This resulted in a $\sim 20\%$ increase in the sample conductivity, and in a ~ 10-meV heighten of the quasi-Fermi level energy with respect to a level position in the case of background irradiation. The photoconductivity kinetics upon laser excitation at different wavelengths was examined before and after irradiation by a series of laser pulses. The kinetic curves $\Delta\sigma/\sigma_0(t)$ are shown in Fig. 10. The shift in the quasi-Fermi level did not change the relative signal amplitude.

Figure 11 exemplifies a diagram illustrating the relationship between characteristic energies in the PbTe(In) spectrum under equilibrium dark conditions and in the presence of background irradiation with different intensities. It is obvious from this diagram that excitation of nonequilibrium carriers by laser pulses is related to the states located in the neighborhood of the quasi-Fermi level.

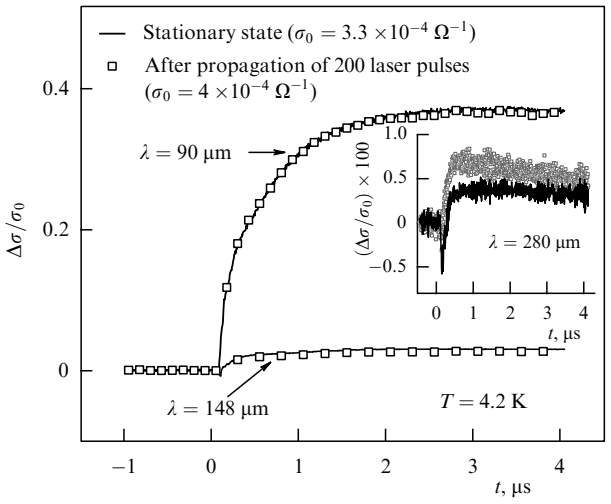

Figure 10. Kinetics of the photoconductivity $\Delta\sigma/\sigma_0$ of a PbTe(In) film irradiated by laser pulses at different wavelengths. Solid curves are obtained at once after sample cooling to 4.2 K. Points correspond to the curve obtained after the propagation of 200 90-μm laser pulses. σ_0 is the conductivity before the laser pulse propagation [27].

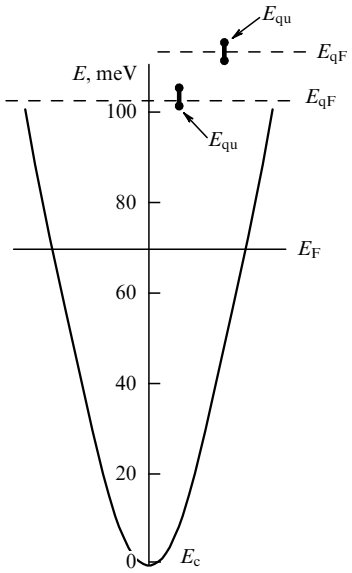

Figure 11. Band diagram of PbTe(In): E_c is the edge of the conduction band, E_F is the position of the stabilized Fermi level in the equilibrium (dark) state of the sample; E_{qF} is the position of the quasi-Fermi level in the presence of background illumination and after the propagation of 200 laser pulses, and E_{qu} is the minimal laser photon energy at which the photoresponse could be detected [27].

A comparison of data for films with different microstructures shows that the formation of the photoresponse in the terahertz wavelength range is sensitive to the type of surface states and film microstructure. In films with a complex microstructure, a number of additional factors affecting their photosensitivity should be taken into account. Thus, it is well known that inhomogeneous high energy-gap semiconductors exhibit IR quenching of persistent photoconductivity [41]. In this case, the energy of an exciting photon should be much lower than the energy gap but comparable to the recombination barrier height. On the contrary, the heating of the electron gas can reduce the activation energy by the mobility threshold, resulting in a photoresponse increase. Each of these factors can considerably depend on the microstructure and character of surface states.

Of most interest are data obtained for a polycrystalline PbTe(In) film. Experiments confirm that solid solutions $Pb_{1-x}Sn_xTe$(In) contain impurity states of a new type which have not been observed in other doped semiconductors so far. The formation mechanism of these states and their microscopic nature are still unclear. Taking into account that one of the analogies of observed effects can be the appearance of a gap in the spectrum of one-electron excitations at the Fermi level in superconductors, it is interesting to study the photoconductivity of solid $Pb_{1-x}Sn_xTe$(In) solutions in a magnetic field by varying an electric current in the sample circuit.

4. Influence of the electric current and magnetic field on the terahertz photoconductivity of solid solutions $Pb_{1-x}Sn_xTe$(In)

The character of changes in the terahertz photoconductivity of solid $Pb_{1-x}Sn_xTe$(In) solutions in the parameter space 'alloy composition–electric current through a sample–magnetic field' was studied in paper [42].

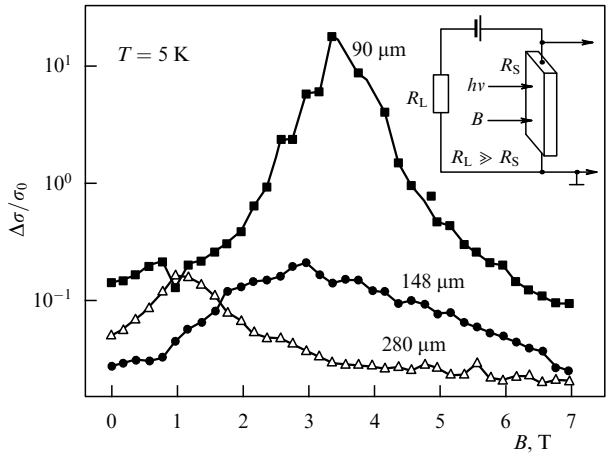

Figure 12. Dependences of the relative positive photoconductivity $\Delta\sigma/\sigma_0$ in a $Pb_{0.75}Sn_{0.25}Te(In)$ alloy on the magnetic field B for different laser radiation wavelengths (indicated alongside the curves) at $T = 5$ K. The inset shows the measurement circuit and experimental geometry [41].

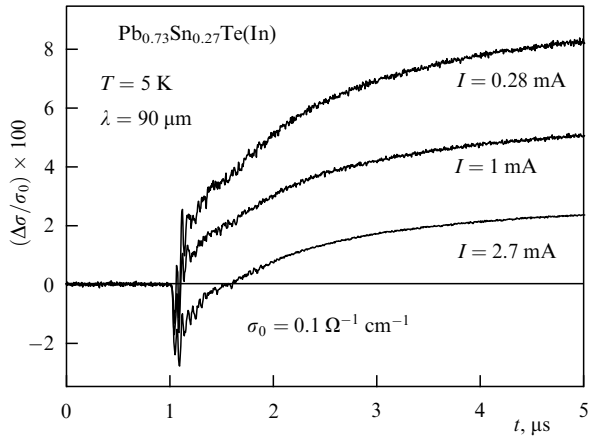

Figure 13. Photoconductivity signal kinetics in a $Pb_{0.73}Sn_{0.27}Te(In)$ alloy measured at different currents flowing through the sample at 5 K. The laser wavelength is 90 μm [41].

Figure 12 depicts the dependence of the relative positive photoresponse $\Delta\sigma/\sigma_0$ (σ_0 is the conductivity in a magnetic field in the initial state of the sample) in the $Pb_{0.75}Sn_{0.25}Te(In)$ alloy on the applied magnetic field for different terahertz laser radiation wavelengths. The magnetic field, like exciting laser radiation, was directed perpendicular to the sample surface (see inset to Fig. 12).

The ratio $\Delta\sigma/\sigma_0$ ($\Delta\sigma$ is the photoconductivity after the end of a laser pulse) demonstrates a change in the concentration of nonequilibrium carriers generated by laser radiation, because the mobility-related contribution to the conductivity is excluded. One can see that the dependence of the relative photoconductivity on the magnetic field has a pronounced maximum. The magnetic field strength corresponding to the maximum is proportional to the laser photon energy. Such a dependence on the magnetic field is quite typical for the cyclotron resonance manifested in the photoconductivity signal (see, for example, Ref. [43]). Assuming that the observed maxima are really related to the cyclotron resonance, we can estimate the effective mass as $m_{\text{eff}} \sim 0.05m_0$. This is close to the real known value of m_{eff} in $Pb_{0.75}Sn_{0.25}Te(In)$ [13]. At the same time, for the cyclotron resonance type effect, a strong dependence of the photoconductivity amplitude on the direction of circular polarization of incident radiation could be expected. However, measurements have shown that such a dependence is lacking. The nature of this effect has not been described in more detail so far.

A series of experiments have been carried out with $Pb_{1-x}Sn_xTe(In)$ samples with the composition changing in the range $0.22 < x < 0.29$. This allowed studying the type of change in the terahertz conductivity for alloys with different configurations of the mutual position of the stabilized Fermi level and the edges of the allowed bands (see Fig. 1). It turned out that the positive terahertz photoconductivity drastically decreased in p-type alloys ($x > 0.26$). At the same time, the negative photoconductivity related to the heating of charge carriers remains. Notice that, during the transition of the stabilized Fermi level through the middle of the forbidden band caused by a change in the alloy composition, the type of photoexcited charge carriers also changes: while for $x \leqslant 0.25$, nonequilibrium electrons are photogenerated, the positive photoconductivity for $x \geqslant 0.26$ corresponds to excitation of nonequilibrium holes [42].

Because the amplitude of the positive persistent photoconductivity in p-type alloys drastically decreases, the negative photoconductivity observed during the laser pulse propagation and related to the heating of charge carriers becomes noticeable against the positive photoconductivity background at the liquid-helium temperature as well. It is important to note that the amplitude of negative photoconductivity is almost independent of the current flowing through the sample, whereas the amplitude of positive persistent photoconductivity decreases several-fold with increasing current by approximately an order of magnitude (Fig. 13). In this case, the current–voltage characteristic of the sample in the initial state is linear.

The data obtained in paper [42] demonstrate that the appearance of local electronic states responsible for the emergence of the terahertz persistent photoconductivity in $Pb_{1-x}Sn_xTe(In)$ alloys is suppressed by the electric field. In addition, it seems likely that the density of such states drastically decreases upon transition to p-type conductivity in alloys with $x \geqslant 0.26$. The local electronic states responsible for terahertz photoconductivity did not decay in magnetic fields in our experiments. One ought not to exclude the explanation that the magnetic fields used in the experiments were not simply strong enough.

5. Features of the photoconductivity of semi-insulating PbTe(V) and PbTe(Ga) samples

Unlike strongly degenerate PbTe(In) alloy, the doping of lead telluride with gallium [10, 14, 44–46] and vanadium [47–50] ensures the formation of a semi-insulating state at low temperatures. Impurity levels stabilizing the location of the Fermi level fall in this case into the forbidden gap. In PbTe(Ga), the Fermi level is stabilized near the middle of the gap by ~ 70 meV below the conduction band bottom E_c; in PbTe(V), it is by ~ 20 meV below E_c (Fig. 14). The majority charge carriers in all cases are electrons.

Despite the fact that the concentrations of charge carriers in both PbTe(Ga) and Pb(Te)(V) samples at low

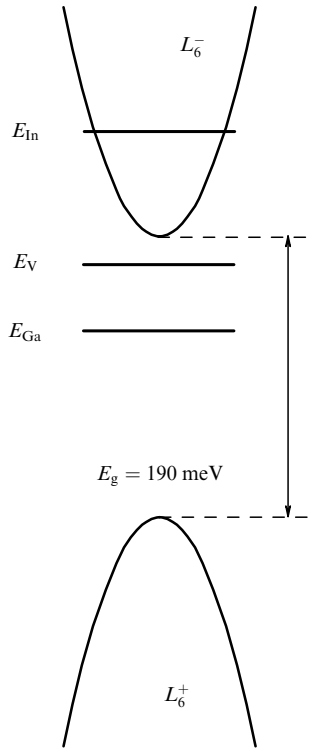

Figure 14. Diagram illustrating the mutual location of the edges of the allowed bands in PbTe and impurity indium, gallium, and vanadium levels stabilizing the position of the Fermi level. L_6^+ and L_6^- are electronic terms forming allowed bands.

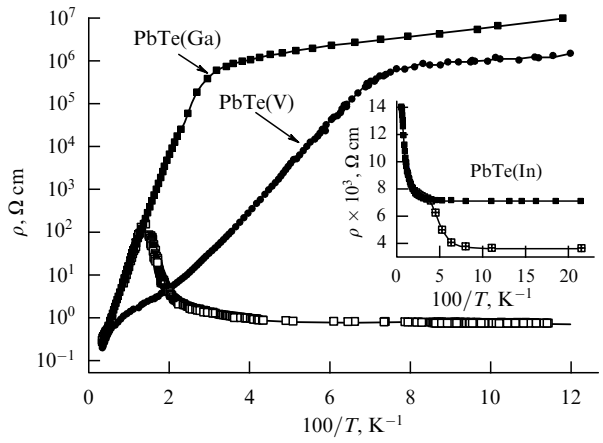

Figure 15. Temperature dependences of the resistivity ρ measured upon background illumination shielding (closed symbols) and upon illumination by white light (open symbols) for PbTe samples doped with Ga, V, and In (inset).

temperatures are close to intrinsic values, persistent photoconductivity was revealed only in PbTe(Ga) for $T < T_c = 80$ K (Fig. 15). PbTe(V) samples remain in the semi-insulating equilibrium state during background irradiation as well.

Because the energy spectrum, basic properties, and theoretical models describing the impurity states of gallium in solid PbTe solutions are described in detail in monograph [10], we will analyze only recent experimental results on the terahertz photoconductivity of PbTe(Ga). The data concerning the properties of PbTe(V) will be considered in more detail.

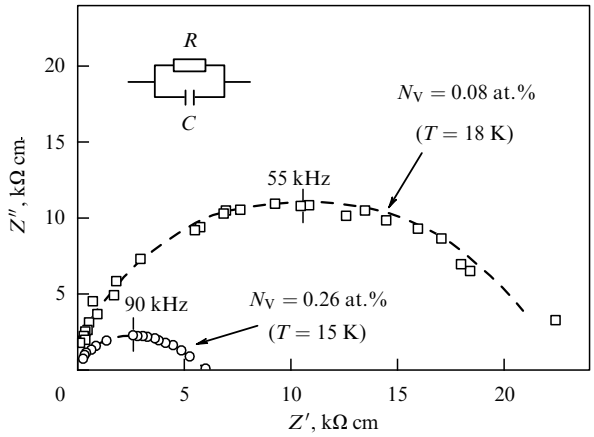

Figure 16. Impedance spectra of PbTe(V) samples with different vanadium contents N_V [48].

5.1 PbTe(V)

5.1.1 Impurity states of vanadium in lead telluride. The Fermi level stabilization effect upon doping with vanadium was most conclusively confirmed in studying the modification of the energy spectrum of solid $Pb_{1-x-y}Sn_xV_yTe$ solutions subjected to hydrostatic compression [49–52]. Energy-spectrum-reconstruction diagrams show that the Fermi-level energy is shifted down along the energy scale both with increasing x and under pressure. Transitions from the semi-insulating to the metal states are observed. Nevertheless, available data [49–52] ambiguously determine the location of the Fermi level in PbTe. According to the studies of a few series of $Pb_{1-x-y}Sn_xV_yTe$ samples, the Fermi level in PbTe(V) can be located in the conduction band [49], directly below its bottom or at a distance of ~ 20 meV from its edge E_c [51, 52]. The latter value best correlates with the results of studying the temperature dependences of the resistance, concentration and mobility of charge carriers in single-crystal PbTe(V) samples with a variable impurity concentration N_V [48]. For a comparatively low doping level ($N_V \leqslant 0.21$ at.%), the properties of samples are completely identical: at $T = 10$ K, the electron concentration does not exceed 10^8 cm^{-3}, while the mobility amounts to 10^5 cm^2 V^{-1} s^{-1}. However, in samples with a maximum vanadium concentration of 0.26 at.% at temperatures below 30 K, the resistivity ρ proves to be considerably lower than in other samples. The decrease in ρ is caused by a drastic (more than an order of magnitude) increase in the electron mobility.

Studies of conductivity in alternating electric fields with frequencies up to 1 MHz revealed that the impedance spectra of samples are represented by one branch, irrespective of the vanadium content in crystals (Fig. 16) [48]. How much these branches correspond to the constant parameters R and C of the equivalent electric circuit can be clearly demonstrated by studying the frequency dependences of the real part σ' of the conductivity calculated directly from experimental data. For a sample with $N_V = 0.08$ at.%, σ' is frequency-independent. A real part of the conductivity of a heavily doped sample with $N_V = 0.26$ at.% increases with f as $\sigma' \sim f^{\alpha}$, where $\alpha = 1.35$. Thus, the equivalent circuit with frequency-independent parameters R and C corresponds only to samples with a low vanadium content. The powerlike frequency dependence of σ' in a sample with the maximum impurity content demonstrates a change in the charge-transfer mechanism with increasing doping level and the possible manifestation of

correlation effects between impurities [53]. The possibility of a considerable broadening of the vanadium impurity level located inside the gap is also pointed out in paper [52].

Magnetic measurements show that the value of the effective magnetic moment per impurity atom corresponds to neither of the known charge states of the vanadium atom. This confirms the manifestation of the mixed valence of the vanadium impurity in lead telluride. The distribution of vanadium atoms over different charge states and the relation between these charge states depend on N_V [48].

5.1.2 Photoconductivity in the terahertz spectral region. Photoconductivity in the terahertz spectral region was studied in PbTe(V) samples with a low impurity content $N_V = 0.08$ at.% [54]. Noticeable photoresponses were observed in the entire temperature range from 8 to 300 K. Typical dependences illustrating the photoconductivity kinetics at different temperatures are illustrated in Fig. 17 for the most long-wavelength 280-μm laser pulse. An important distinctive feature of these data is that the maximum amplitude $\Delta\sigma_{max}$ of the photoconductivity increases by approximately three orders of magnitude with increasing temperature to 300 K. In this case, the maximum relative change $\Delta\sigma_{max}/\sigma_0$ in the conductivity decreases with temperature approximately by an order of magnitude [54].

A comparison of the maximum photoresponse amplitude $\Delta\sigma_{max}$ with the dark conductivity σ_0 reveals that changes in these parameters are correlated (Fig. 18). The increase in σ_0 with temperature is caused by the increase in the concentration of free electrons. The increase in the positive photoconductivity in the presence of constant background irradiation can be caused only by the increase in the generation rate of non-

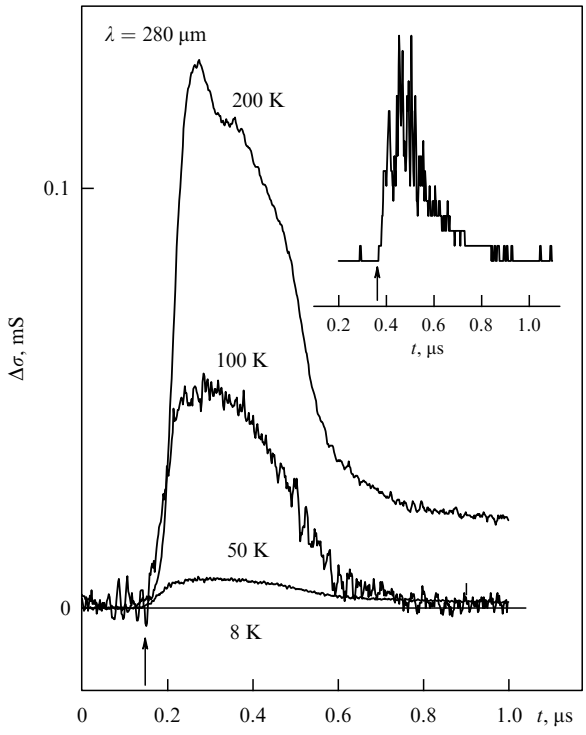

Figure 17. Changes in the photoconductivity of a PbTe(In) sample with $N_V = 0.08$ at.% during propagation of 280-μm laser pulses at different temperatures (indicated alongside the curves). The arrows mark the instant of time corresponding to the beginning of pulse propagation. The inset shows the laser pulse shape [54].

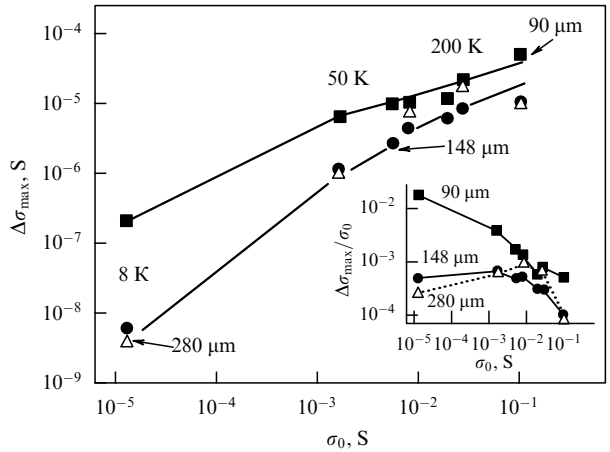

Figure 18. Dependence of the maximum photoconductivity $\Delta\sigma_{max}$ on the conductivity σ_0 of a sample in the initial state. The corresponding temperatures and laser pulse wavelengths are indicated in the figure. The inset shows the dependence of the relative conductivity $\Delta\sigma_{max}/\sigma_0$ on σ_0. The data are calculated per photon flux of 10^{24} s^{-1} [54].

equilibrium charge carriers, because their mobility decreases with increasing temperature. The increase in the generation rate is most likely caused by the reconstruction of the energy spectrum of PbTe(V) with changing temperature. According to estimates made in paper [51] for solid $Pb_{1-x-y}Sn_xV_yTe$ solutions, the impurity vanadium level approaches the bottom of the conduction band at a rate of about 0.1 meV K^{-1}. Thus, as temperature is increasing, laser photon energies can become comparable to the thermal activation energy of carriers from impurity centers.

In the low-temperature region, the terahertz photon energy is considerably lower than the thermal activation energy of impurity states responsible for the Fermi-level stabilization. This leads to a drastic decrease in the photoresponse amplitude, especially for small photon energies. One of the possible factors responsible for the presence of a weak positive photoresponse is a considerable broadening of the impurity level or formation of an impurity band. Here, the electronic states located slightly above the Fermi level can be weakly thermally populated in the impurity band, even in the absence of terahertz radiation. Electrons can be generated into the conduction band by terahertz radiation namely from these states, whose populations exponentially increase with temperature, thus increasing the photoresponse amplitude. In this case, the thermal activation energy of carriers from the impurity band decreases, which also favors the increase in the amplitude of the absolute value of the photoconductivity signal.

At temperatures above 100 K, the absolute photoresponse amplitude does not noticeably depend on the laser pulse wavelength. It is in this temperature region that the exciting photon energies become comparable to the distance from the Fermi level to E_c. These conclusions agree with those made in Refs [51, 52]. At the same time, one ought not to exclude the explanation that the effect observed is caused by phonon-induced tunneling under the action of high-power terahertz radiation [55].

5.2 Terahertz photoconductivity of PbTe(Ga) exposed to variable background radiation

The spectra and kinetics of photoconductivity in PbTe(Ga) samples, notably in the terahertz spectral region, were studied in papers [56–59].

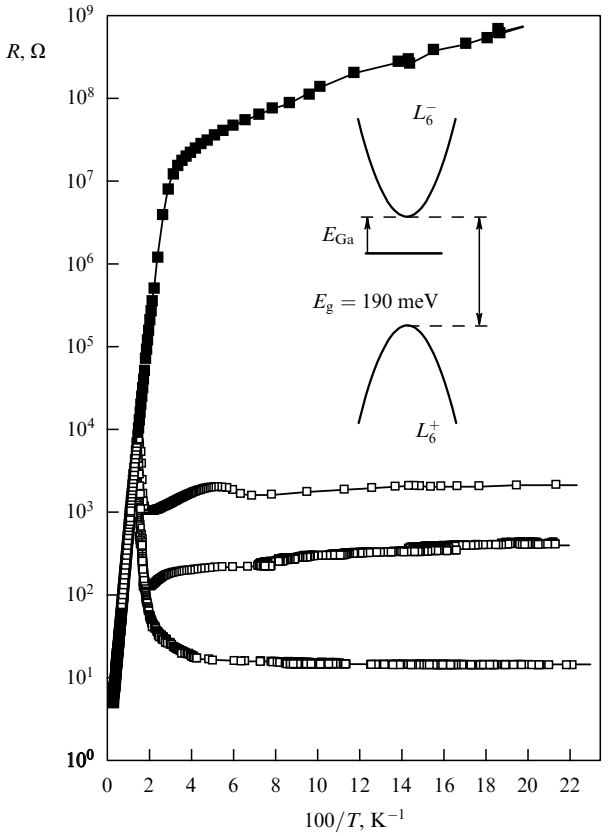

Figure 19. Temperature dependences of the resistance of a PbTe(Ga) sample measured upon background illumination shielding (closed symbols) and at different excitation levels (open symbols) induced by external illumination. L_6^+ and L_6^- are electronic terms forming allowed bands [59].

One of the important features of gallium-doped lead telluride is the possibility of changing the conductivity of the sample in a rather wide range, even in the presence of background irradiation. In this case, quasistationary states at low temperatures remain stable for an indefinitely long time after switching off additional irradiation (Fig. 19). Studies of the photoconductivity of PbTe(Ga) in the terahertz spectral region have shown that not only the kinetics but also the sign of the photoconductivity signal depend on the initial excitation level (the quasi-Fermi-level location in the initial state of the sample before laser pulse propagation). Under conditions of weak background irradiation, the terahertz conductivity is negative in the entire temperature range from 4.2 to 100 K (Fig. 20). An increase in the initial conductivity σ_0 caused by additional irradiation with white light gives rise to persistent positive photoconductivity in the terahertz region. The photoresponse kinetics in this case are similar to those observed in PbTe(In) films. Thus, to obtain a positive terahertz photoconductivity in PbTe(Ga), a high enough density of states at the quasi-Fermi level is required. This result suggests that there is a unified mechanism responsible for the formation of states 'attached' to the quasi-Fermi level in lead telluride doped with group III elements exhibiting a variable valence with the difference in charge states of two unit charges. It is important that in PbTe(V), where impurity states differ only by the unit charge [48], the formation mechanism of the positive photoresponse in the terahertz spectral region is qualitatively distinct.

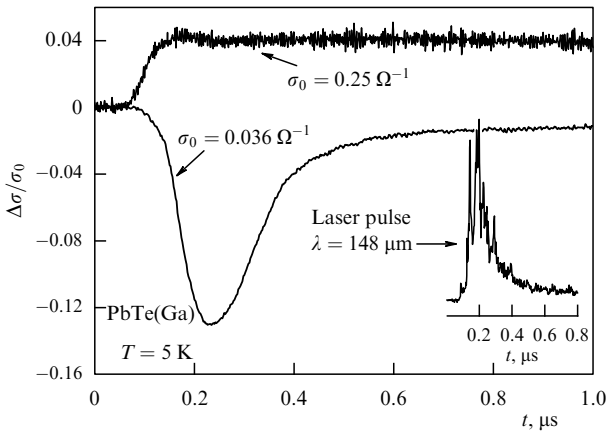

Figure 20. Kinetics of the relative photoconductivity signal of a PbTe(Ga) sample during propagation of a 148-μm laser pulse for states with different initial conductivities σ_0. The inset shows the time profile of the laser pulse [59].

6. Conclusions

The study of photoelectric effects induced by terahertz radiation in lead telluride alloys doped with In and Ga has allowed us to substantially reconsider concepts about the physics of local electronic states in this class of semiconductors. If we interpret the results obtained assuming that electrons are excited from one-particle local states, it is necessary to recognize that special local states appear, which are 'attached' to the quasi-Fermi level and are shifted together with it, unlike traditional impurity states having rather distinct location in the energy spectrum of a material. These unusual local states are responsible for the appearance of the persistent positive photoconductivity in the terahertz spectral region and the emergence of the unique monopolar photoelectromagnetic effect induced by high-power terahertz laser radiation [60].

Aside from nontrivial physics, the unique properties of doped narrow-gap lead telluride-based semiconductors are quite promising for manufacturing highly sensitive photodetectors in the terahertz range.

The terahertz range of electromagnetic waves is one of the least mastered. At the same time, a great number of important problems in many research fields involve the study of radiation just in the terahertz range. Examples cover biomedical applications, safety systems, space research, and many others.

Most of the modern spectroscopic systems in the terahertz range use the active location method, in which the object under study is irradiated by a high-power terahertz laser pulse and a signal reflected from or transmitted through the object is analyzed. Passive systems based on terahertz radiation emitted by the object itself are virtually absent. The only exception known to us is photodetector systems for spaceborne terahertz astronomy. However, these unique devices require profound cooling to ultralow temperatures of about 100 mK. The semiconductors studied here can become promising materials for passive location at operating temperatures of about 5–7 K.

The effect of terahertz persistent photoconductivity observed in $Pb_{1-x}Sn_xTe$(In) alloys provides a kind of 'internal integration' of the incident electromagnetic radiation. This is important because it is this factor that ensures the increase in the signal-to-noise ratio in photodetectors. At the

same time, to create a real photodetector, it is necessary to develop a method for the rapid quenching of persistent photoconductivity. In Ref. [61], a technique was proposed for the rapid (~ 1 μs) drop in the accumulated signal, thus providing the operation of the device in the mode of periodic accumulation of the photoconductivity signal followed by its rapid drop. Based on this method, an operation mode of the photodetector was realized in which radiofrequency pulses applied to the contacts of the semiconductor periodically suppressed the persistent photoconductivity. In this case, the photoconductivity signal has a saw-tooth shape, with the 'saw' amplitude corresponding to the intensity and spectral composition of radiation incident on the photodetector [62]. Recent studies have shown that, according to preliminary estimates, the sensitivity of terahertz $Pb_{1-x}Sn_xTe(In)$-based photodetectors are at least comparable to that of analogs known throughout the world [63, 64]. We can expect that, due to their comparatively high operating temperature, systems based on doped solid lead telluride solutions will find wide 'earthly' and space applications.

Acknowledgments.
The authors are grateful to S D Ganichev and V V Bel'kov for many useful discussions. The work was partially supported by DFG, DAAD, IB's Linkage Grant from BMBF at DLR, the Russian Foundation for Basic Research (grant Nos 14-02-00250-a and 13-02-00580-a) and the Development Program of Lomonosov Moscow State University.

References

1. Fu L *Phys. Rev. Lett.* **106** 106802 (2011)
2. Dziawa P et al. *Nature Mater.* **11** 1023 (2012)
3. Tanaka Y et al. *Phys. Rev. B* **87** 155105 (2013)
4. Mahan G D, Sofo J O *Proc. Natl. Acad. Sci. USA* **93** 7436 (1996)
5. Heremans J P et al. *Science* **321** 554 (2008)
6. Heremans J P, Wiendlocha B, Chamoire A M *Energy Environ. Sci.* **5** 5510 (2012)
7. Jovovic V et al. *J. Appl. Phys.* **103** 053710 (2008)
8. Dmitriev A V, Zvyagin I P *Phys. Usp.* **53** 789 (2010) *Usp. Fiz. Nauk* **180** 821 (2010)
9. Fu H, Tsang S-W *Nanoscale* **4** 2187 (2012)
10. Khokhlov D (Ed.) *Lead Chalcogenides: Physics & Applications* (New York: Taylor & Francis, 2003)
11. Rahim M et al. *Opt. Lett.* **33** 3010 (2008)
12. Kaidanov V I, Ravich Yu I *Sov. Phys. Usp.* **28** 31 (1985); *Usp. Fiz. Nauk* **145** 51 (1985)
13. Nimtz G, Schlicht B, in *Narrow-Gap Semiconductors* (Springer Tracts in Modern Physics, Vol. 98, Ed. G Hohler) (Berlin: Springer-Verlag, 1983)
14. Volkov B A, Ryabova L I, Khokhlov D R *Phys. Usp.* **45** 819 (2002); *Usp. Fiz. Nauk* **172** 875 (2002)
15. Volkov B A, Ruchaiskii O M *JETP Lett.* **62** 217 (1995); *Pis'ma Zh. Eksp. Teor. Fiz.* **62** 205 (1995)
16. Akimov B A et al. *Sov. Phys. Semicond.* **13** 441 (1979); *Fiz. Tekh. Poluprovodn.* **13** 752 (1979)
17. Khokhlov D R et al. *Appl. Phys. Lett.* **76** 2835 (2000)
18. Kazanskii A G, Richards P L, Haller E E *Appl. Phys. Lett.* **31** 496 (1977)
19. Ryabova L I, Khokhlov D R *JETP Lett.* **97** 720 (2013); *Pis'ma Zh. Eksp. Teor. Fiz.* **97** 825 (2013);
20. Schneider P et al. *J. Appl. Phys.* **96** 420 (2004)
21. Ganichev S D et al. *Phys. Rev. Lett.* **80** 2409 (1998)
22. Ganichev S D, Terent'ev Ya V, Yaroshetskii I D *Sov. Tech. Phys. Lett.* **11** 20 (1985); *Pis'ma Zh. Tekh. Fiz.* **11** 46 (1985)
23. Ziemann E et al. *J. Appl. Phys.* **87** 3843 (2000)
24. Galeeva A V et al. *JETP Lett.* **91** 35 (2010); *Pis'ma Zh. Eksp. Teor. Fiz.* **91** 37 (2010)
25. Khokhlov D et al. *Appl. Phys. Lett.* **93** 264103 (2008)
26. Ryabova L I et al., in *Trudy XVII Mezhdunarodnogo Simpoziuma "Nanofizika i Nanoelektronika", Nizhnii Novgorod, 11–15 Marta 2013* (Proc. of the XVII Intern. Symp. on Nanophysics and Nanoelectronics, Nizhny Novgorod, 11–15 March 2013) Vol. 2 (Nizhny Novgorod: Institute of Physics of Microstructures, 2013) p. 635
27. Chernichkin V I et al. *Europhys. Lett.* **100** 17008 (2012)
28. Dashevsky Z, Kreizman R, Dariel M P *J. Appl. Phys.* **98** 094309 (2005)
29. Neustroev L N, Osipov V V *Fiz. Tekh. Poluprovodn.* **20** 34 (1986)
30. Dashevsky Z et al. *J. Nanoelectron. Optoelectron.* **4** 296 (2009)
31. Dashevsky Z, in *Handbook of Semiconductor Nanostructures and Nanodevices* Vol. 4 (Ed. A A Balandin, K L Wang) (Stevenson Ranch, Calif.: American Scientific Publ., 2006) Ch. 11
32. Komissarova T et al. *Phys. Rev. B* **75** 195326 (2007)
33. Dobrovolsky A A et al. *Semiconductors* **43** 253 (2009); *Fiz. Tekh. Poluprovodn.* **43** 265 (2009)
34. Dobrovolsky A A et al. *Semicond. Sci. Technol.* **24** 075010 (2009)
35. Chernichkin V I et al. *Semiconductors* **45** 1474 (2011); *Fiz. Tekh. Poluprovodn.* **45** 1533 (2011)
36. Dobrovolsky A et al. *Phys. Status Solidi C* **7** 869 (2010)
37. Dobrovolsky A et al. *J. Phys. Conf. Ser.* **150** 022009 (2009)
38. Dobrovolsky A et al. *Int. J. Mater. Res.* **100** 1252 (2009)
39. Akimov B A et al. *Sov. Phys. Semicond.* **17** 1021 (1983); *Fiz. Tekh. Poluprovodn.* **17** 1604 (1983)
40. Ryabova L et al. *Proc. SPIE* **8439** 84391H-1 (2012)
41. Sheinkman M K, Shik A Ya *Sov. Phys. Semicond.* **10** 128 (1976); *Fiz. Tekh. Poluprovodn.* **10** 209 (1976)
42. Ryabova L I et al. *JETP Lett.* **97** 525 (2013); *Pis'ma Zh. Eksp. Teor. Fiz.* **97** 607 (2013)
43. Kvon Z-D et al. *Physica E* **40** 1885 (2008)
44. Akimov B A et al. *Phys. Lett. A* **88** 483 (1982)
45. Ryabova L I, Khokhlov D R *JETP Lett.* **80** 133 (2004); *Pis'ma Zh. Eksp. Teor. Fiz.* **80** 143 (2004)
46. Skipetrov E P et al. *J. Cryst. Growth* **210** 292 (2000)
47. Skipetrov E P et al. *Mold. J. Phys. Sci.* 8 63 (2009)
48. Artamkin A I et al. *Semiconductors* **44** 1543 (2010); *Fiz. Tekh. Poluprovodn.* **44** 1591 (2010)
49. Skipetrov E P et al. *Physica B* **404** 5262 (2009)
50. Skipetrov E P et al. *Low Temp. Phys.* **39** 76 (2013); *Fiz. Nizk. Temp.* **39** 98 (2013)
51. Skipetrov E P et al. *Semicond. Sci. Technol.* **27** 015019 (2012)
52. Skipetrov et al. *Semiconductors* **46** 741 (2012); *Fiz. Tekh. Poluprovodn.* **46** 761 (2012)
53. Mott N F, Davis E A *Electronic Processes in Non-Crystalline Materials* (Oxford: Clarendon Press, 1979); Translated into Russian: *Elektronnye Protsessy v Nekristallicheskikh Veshchestvakh* Vol. 1 (Moscow: Mir, 1982)
54. Artamkin A I et al. *Semiconductors* **47** 319 (2013); *Fiz. Tekh. Poluprovodn.* **47** 293 (2013)
55. Ganichev S D, Prettl W, Huggard P G *Phys. Rev. Lett.* **71** 3882 (1993)
56. Belogorokhov A I et al. *JETP Lett.* **72** 123 (2000); *Pis'ma Zh. Eksp. Teor. Fiz.* **72** 178 (2000)
57. Romcevic N et al. *Infrared Phys. Technol.* **40** 453 (1999)
58. Romcevic M et al. *J. Phys. Condens. Matter* **12** 8737 (2000)
59. Egorova S G et al. *J. Alloys Comp.* **615** 375 (2014)
60. Chernichkin V I et al. *Semicond. Sci. Technol.* **27** 035011 (2012)
61. Akimov B A, Khokhlov D R *Semicond. Sci. Technol.* **8** S349 (1993)
62. Chesnokov S N et al. *Infrared Phys.* **35** 23 (1994)
63. Dolzhenko D et al. *Proc. SPIE* **8452** 84520W (2012)
64. Khokhlov D R, in *Abstracts of ICONO/LAT 2013, Moscow, 18–22 June 2013* (2013) p. 108